A method for multi-resolution characterization on porous surfaces by using a laser confocal scanning microscope

Yibo Zou, Markus Kaestner, Eduard Reithmeier

Institute of Measurement and Automatic Control, Leibniz University of Hannover, Nienburger Str. 17, 30167, Hannover, Germany

Abstract

In this paper, a new method for multi-resolution characterization is introduced to analyze porous surfaces on cylinder liners. The main purpose of this new approach is to investigate the influence of resolution and magnification of different optical lenses on measuring the 3D geometry of pores based on 3D microscopy topographical surface metrology. Two optical sensors (20x lens and 50x lens) have been applied to acquire the porous surface data for the primal investigation. A feature-based image matching algorithm is introduced for the purpose of registering identical micro structures in different datasets with different pixel resolutions. The correlation between the sensor's resolution and the numerical parameters' values regarding the pores geometry is studied statistically. Finally, the preliminary results of multi-resolution characterization are presented and the impact of using a sensor with higher resolution on measuring the same object is discussed.

Keywords: Multi-resolution, surface registration, characterization, porous surface

1. Introduction

In automobile industry, thermal spray coating plays an important role in liquid-lubricated high performance contact pairs, e.g. cylinder liners in combustion engines, dealing with porous material layers to optimize the tribological behaviour and lubrication in view of fuel efficiency [1][2][3]. In order to investigate this functional relevant coating, a comprehensive surface characterization should be developed with the help of 3D optical microscopy metrology. Subsequently, a quantitative analysis of numerical parameters combined with tribological tests may imply significant correlations, which can give feedback to the manufacturing process to realize a better quality control.

Traditionally, metrologists have to face the fundamental problem of selecting an appropriate lens of a microscope to conduct data acquisition: using a lens with a low magnification not only leads to a faster areal data acquisition but can also obtain a larger field of view.However, due to the limited pixel resolution of the CCD sensor, it lacks in further details of the micro structures. On the other hand, a dataset, which is acquired by using a lens with a higher magnification, usually provides a more detailed surface nature. But it is more time-consuming regarding to the aspects of data acquisition and data post processing. For this reason, a multi-resolution characterization method is developed here, in order to understand the influences of switching lenses on characterization results. Afterwards, the correlation analysis between lens' resolution and numerical parameters of micro structures is carried out to answer the questions e.g. which parameters are invariant to different resolutions, which are variant to different resolutions and how their values are fluctuating as different lenses have been applied.

By this way, a rapid characterization can be realized: in the case of the parameters that are invariant to sensor resolutions, a lens with low resolution can be selected to conduct surface measurement; while for those parameters, which are variant to different sensor resolutions, the relation between the numerical values and sensor resolutions can be analyzed and then recorded. Hence, a fast characterization can be achieved by such a manner that the high resolution sensor-based numerical parameters are estimated by them that are measured with the sensors with a lower resolution.

The aim of this article is to introduce a method to perform a multiscale surface characterization. Porous surfaces are used as specimen and are investigated in this paper due to their importance in today's industry as described above. The study focuses on the impact of the different sensors' resolutions on the measurement of pores' 3D geometry information. During the surface data acquisition, a 20x lens and a 50x lens of a confocal laser scanning microscope have been applied to achieve different scales of the datasets. The data processing and post characterization are based on digital image analysis techniques.

2. Material and Methods

2.1. Sample preparation and experiment setup

In this study, a thermal spray coating process, in which a cast iron substrate was coated with plasma torch F4MB (Sulzer Metro, Wohlen/ Switzerland), is used to prepare the samples. In the final machining, honing processing was carried out with diamond ledges to produce a porous surface [4][5].

Surface textures are measured by a laser confocal scanning microscope (Keyence VK200), which provides not only 3D topographical height maps but also surface intensity maps. The

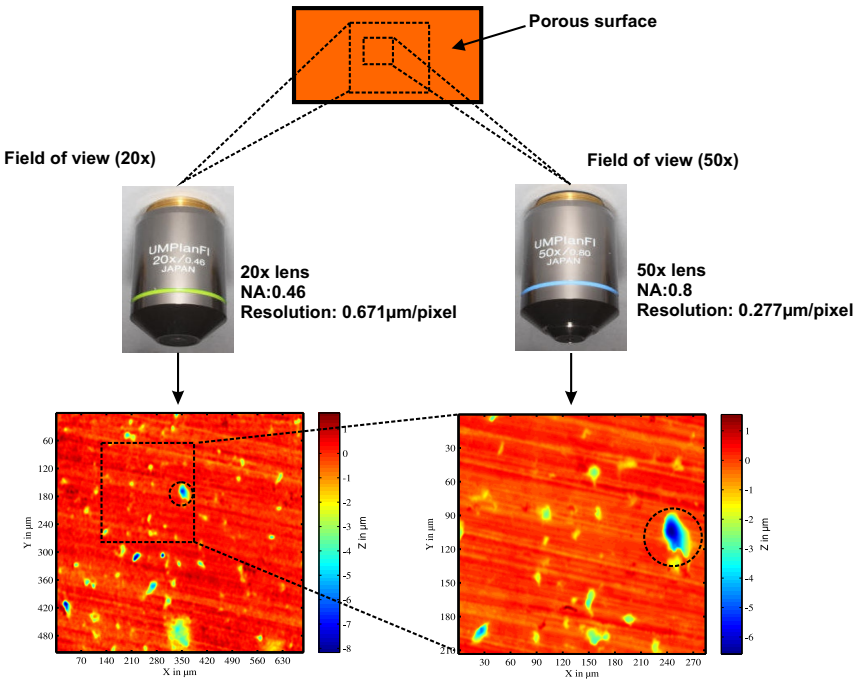

Figure 1: Experiment setup for the multi-resolution data acquisition.

strategy for the multi-resolution data acquisition in this study is briefly presented in Fig.1: A 20x lens with 0.677 µm/pixel resolution and a 50x lens with 0.227 µm/ pixel resolution are successively used to obtain areal surface data. It must be emphasized that an overlapping surface area has to be guaranteed, so that the identical pores can be observed in the different datasets (see Fig. 1).

2.2. Registration of datasets based on surface features

2.2.1. Registration strategy

A direct comparison of the 3D geometry of identical pores in different datasets needs spatial surface localization. Such a problem is often considered as 3D surface registration. During the past decade, much effort on automatic matching of complex surfaces has been made in order to build a global CAD coordinate system. The matching procedures are usually divided into two steps: coarse matching and final matching [6]. For the coarse matching, some similar features and descriptors (e.g. color texture information [7], moments [8] and spin image [9]) of surfaces are firstly defined and then extracted. Afterwards, a fine matching follows the coarse registration. The most common studied approach is the Iterated Closest Point (ICP) algorithm [10][11]. The approximation and convergence of those strategies depend mainly on the complexity of the surface geometry and the data acquisition methods.

However, according to the characteristics of the planar form of the specimen as well as the dataset model in CCD sensor with a fixed lateral sample spacing, it is possible to develop a new strategy to tackle the registration problem. The basic idea behind this new approach can be summarized as follows: firstly, both obtained intensity datasets are extracted as extra information converting to grayscale images. In the second step, the SURF (Speeded Up Robust Features) algorithm, which is a feature-based image registration method, is applied to both grayscale images for the purpose of determining the affine transformation between both image coordinates. Thenceforth, a data pre-processing including leveling, filtering, segmentation etc. is proceeded on the corresponding topographical height maps. Finally, with the help of the extracted affine transformation above, registration and spatial localization of micro structures can be achieved on 3D height maps.

2.2.2. Implementation of the SURF algorithm

The SURF algorithm is based on scale space theory [12][13]. It detects local extrema as feature points on objects in images, where the feature points are determined by a hessian based blob detector:

$$\mathrm{H}(\mathbf{x},\sigma) = \begin{bmatrix} L_{xx}(\mathbf{x},\sigma) & L_{xy}(\mathbf{x},\sigma) \\ L_{xy}(\mathbf{x},\sigma) & L_{yy}(\mathbf{x},\sigma) \end{bmatrix} \tag{1}$$

where

$$L_{xx}(\mathbf{x},\sigma) = I(\mathbf{x}) * \frac{\partial^2}{\partial x^2} g(\sigma) \tag{2}$$

$$L_{xy}(\mathbf{x},\sigma) = I(\mathbf{x}) * \frac{\partial^2}{\partial xy} g(\sigma) \tag{3}$$

$L_{xx}(\mathbf{x},\sigma)$ is the convolution of the image $I(\mathbf{x})$ with the second derivative of the Gaussian kernel. In SURF algorithm, the box filter kernel D is applied to approximate this second order Gaussian kernel for the purpose of improving the efficiency

[14]. Thus, the feature points is determined by the determinant of the approximated Hessian matrix (see Fig.2 and Fig. 3):

$$Det(H) = D_{xx}D_{xy} - (wD_{xy})^2, \tag{4}$$

where the approximated kernels D_{xx} and D_{xy} correspond to the kernels $L_{xx}(\mathbf{x}, \sigma)$ and $L_{xy}(\mathbf{x}, \sigma)$. w is a weighting factor to compensate the approximation with box filter kernels.

In order to improve the computational speed, the image $I(\mathbf{x})$ in SURF is approximated by an integral form, where each point $\mathbf{x} = (x, y)^T$ stores the sum of all the pixels in a rectangular area between the starting point and $\mathbf{x}$:

$$I(\mathbf{x}) = \sum_{i=0}^{i\leq x} \sum_{j=0}^{j\leq y} I(x, y) \tag{5}$$

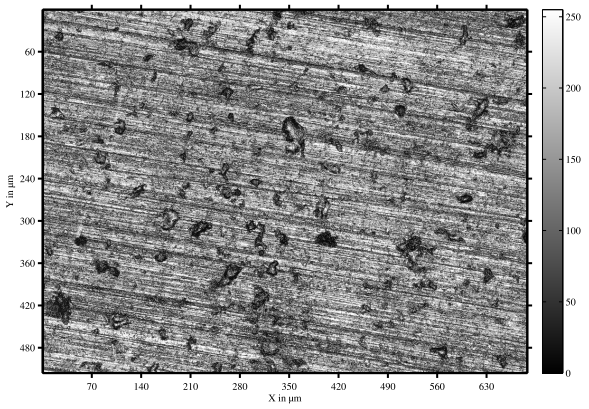

Figure 2: Original gray image of a porous surface taken by 20x lens

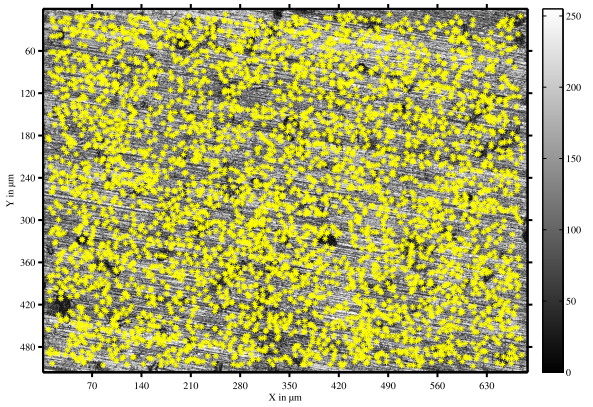

Figure 3: Feature point detection based on Hessian matrix

After that, the image combining with feature points is presented in scale space with a pyramid structure to achieve scale invariance. Each feature point is characterized by a distinctive descriptor using its 64 neighbors' gradient information. The purpose of the descriptor is to achieve invariance against translation, rotation and shear. Finally, the best matching points can be found by ranking all the feature points' descriptors. In Fig. 4, the image matching is visualized by aligned lines based on the best matching feature points after implementing the SURF algorithm. Here, the two grayscale images have the same image size (1024x768), but in different resolutions as illustrated above (on the left: 20x grayscale image; on the right: 50x grayscale image). It should be noted that this method is usually applicable only in the scope of grayscale monochrome images [14] [15].

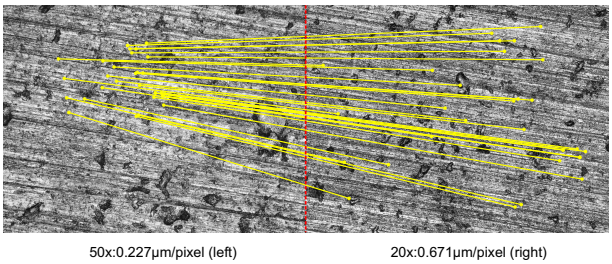

Figure 4: Feature points matching between two gray images in two different scales

The image warp transformation can be extracted by the coordinates of the best matching points in each image. This can be summarized in an affine transformation [16]:

$$\begin{bmatrix} x' \\ y' \\ 1 \end{bmatrix} = \begin{bmatrix} a & b & t_x \\ c & d & t_y \\ 0 & 0 & 1 \end{bmatrix} \begin{bmatrix} x \\ y \\ 1 \end{bmatrix} \tag{6}$$

where t_x and t_y depict the translation and the matrix $\begin{bmatrix} a & b \\ c & d \end{bmatrix}$ on the top left consists of the rotation, scale and shear transform between the image coordinates. Before we apply the affine transformation to the both corresponding topographical height maps, a data pre-processing is conducted. Firstly, both topographical datasets (50x height map and 20x height map) are leveled by using robust least square fitting in order to eliminate the surface form. Subsequently, the leveled surfaces are filtered by using a Gaussian filter with the same cut-off length. After that, the filtered height maps are segmented into a binary image by using a threshhold method with the same thresh value. Finally, the pores within respective resolution are presented with the help of a binary map (see Fig. 5). On the basis of the extracted affine transformation above, a bounding box around a pore e.g. on the left dataset (50x) is drawn in Fig. 5 in order to validate the transformation, the correspondent bounding box is then calculated automatically and located around the identical pore in the right dataset (20x) in Fig. 5. In this manner, we have realized spatial registration of identical pores within the different datasets. In the next step, we extract the local 3D geometry of pores inside the bounding boxes above, where the data processing is based on both pre-processed topographical datasets. The purpose is to unveil the statistical difference regarding to the numerical parameters of the pores in different scales.

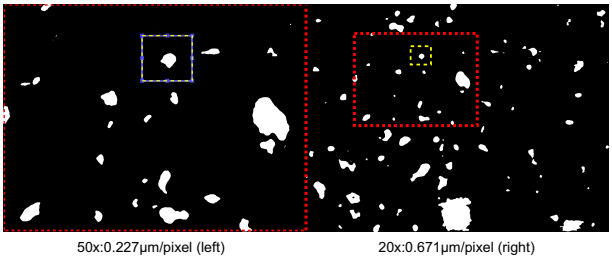

Figure 5: Validation of registration via boundingbox in binary image

2.3. Numerical parameters

In this preliminary study, six numerical parameters (area, volume, equivalent diameter, eccentricity, 95 % maximal depth and mean depth of pore) were initially investigated to study the difference relating to the pores' 3D geometry under different resolutions. The calculation of those parameters is based on image processing and pixel analysis with help of Matlab image processing toolbox. The definition of each parameter is listed in Table 1.

Subsequently, a comparative study of the numerical parameters under the two different resolutions can be achieved by selecting a series of identical pores (250 identical pores have been used in this study for statistical analysis). A deviation histogram has been applied to reveal the statistical difference, which is defined by:

$$Hist\ (\textbf{parameter 50x} - \textbf{parameter 20x}) \tag{7}$$

where **parameter 50x** is a vector including all the six parameters in small scale and **parameter 20x** is also a vector, which consists of all the extracted parameters from 20x lens' datasets.

3. Characterization results

In Fig. 6, the deviation histograms provide a clear overview over the statistical difference: in the case of parameters A, V and D, their deviation histograms are totally shifted to the right side of the axis of $x = 0$, which shows that the values have been increased by using the lens with a higher resolution (50x). However, it is worthy to note that the deviation histogram of the parameter E exhibits a quasi gauss form distribution symmetrically to the axis ($x = 0$). This implies that the vast majority of pores keep the same morphological shape when they are measured by using another optical lens. Moreover, the vertical relevant parameters such as $H_{95\%}$ and H_{mean} are also influenced. As shown in Fig. 6, their deviation histograms are likewise shifted to the right site of the axis $x = 0$, although the tendency is less strong than the lateral relevant parameters in term of area, volume and equivalent diameter.

For the purpose of evaluating the increasing ratio for each parameter (except eccentricity), the average increasing rate (AIR) is investigated based on the deviation histograms above, which is defined by:

$$\textbf{AIR} = \frac{\textbf{parameter 50x} - \textbf{parameter 20x}}{\textbf{parameter 20x}} \tag{8}$$

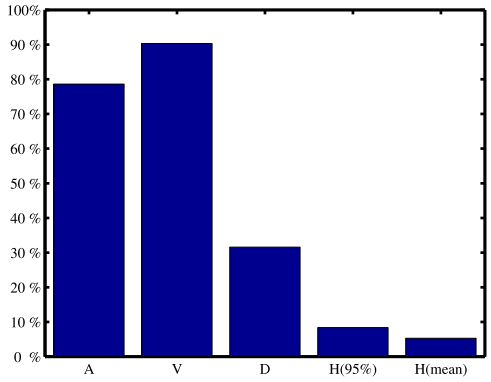

Figure 7: Average increasing rate

Fig. 7 gives a clue how strongly each parameter varies because of rising the sensor's resolution at a first glance. Obviously, all investigated parameters' numerical values have been increased as a result of using the lens 50x. In addition to that, the influences on lateral relevant parameters are more intensive than on the vertical relevant parameters. For instance, the AIR of the parameter A (78.6%) is much larger than the AIR of the parameter $H_{95\%}$ (8.4%).

In order to conduct a more detailed survey, each parameter's numerical value and its associated increasing rate were rearranged as ascending sort. The relative increasing rate (RIR) is defined by:

$$\textbf{RIR} = sort\ (\frac{\textbf{parameter 50x} - \textbf{parameter 20x}}{\textbf{parameter 20x}}) \tag{9}$$

Thus, an error bar chart is used for the purpose of studying the relative increasing rate (RIR) for each parameter. Fig. 8 provides more details about the distribution of the increasing rate, which is correlated to each single parameter's value. Based on this, some useful conclusions can be drawn. Firstly, the smaller the area that a pore holds, the greater is the impact of the high resolution lens (50x), as shown in Fig. 8a. That is to say, the pores with smaller sizes can be more accurately acquired and characterized by a lens with a high resolution.

Secondly, the RIR (e.g. in Fig. 8a) becomes more and more stable as the pore's size gets larger and it can also be observed that the RIR is converging to a constant when a pore is large enough. Thirdly, the error variance becomes larger as the pore's size decreases, which indicates a larger uncertainty when measuring those small pores by using a lens (20x) with a lower resolution (see Fig. 8a).

A similar tendency can also be found in the other investigated parameters. Fig.8b-d provide a clear interpretation of the relation between the RIR and the sorted parameter values. Moreover, this evidence can be proven not only in lateral relevant parameters (e.g see Fig. 8b), but also in depth relevant parameters (e.g see Fig. 8c). Based on these results, we convince that choosing a lens with a higher resolution does affect the characterization results and can provide more details regarding to the pore's 3D geometrical parameter. Furthermore, the impact on

Parameter	Definition	Notes
Area	$A = \sum_{x,y} R_i \cdot x_{resolution} \cdot y_{resolution}$	R_i: region strucure of pores
Volume	$V = \sum_{x,y} \lvert M_{R_i} \rvert \cdot x_{resolution} \cdot y_{resolution}$	M_{R_i}: height matrix of region
Equivalent Diameter	$D = \sqrt{\frac{4A}{\pi}}$	
Eccentricity	$E = \sqrt{1 - (b/a)^2}$	a,b: length of major and minor axis
95% maximal depth	$H_{95\%} = 0.95 \cdot \lvert M_{R_i} \rvert$	
Mean depth	$H_{mean} = Mean(\lvert M_{R_i} \rvert)$	

Table 1: Definition of numerical parameters of pore micro structures

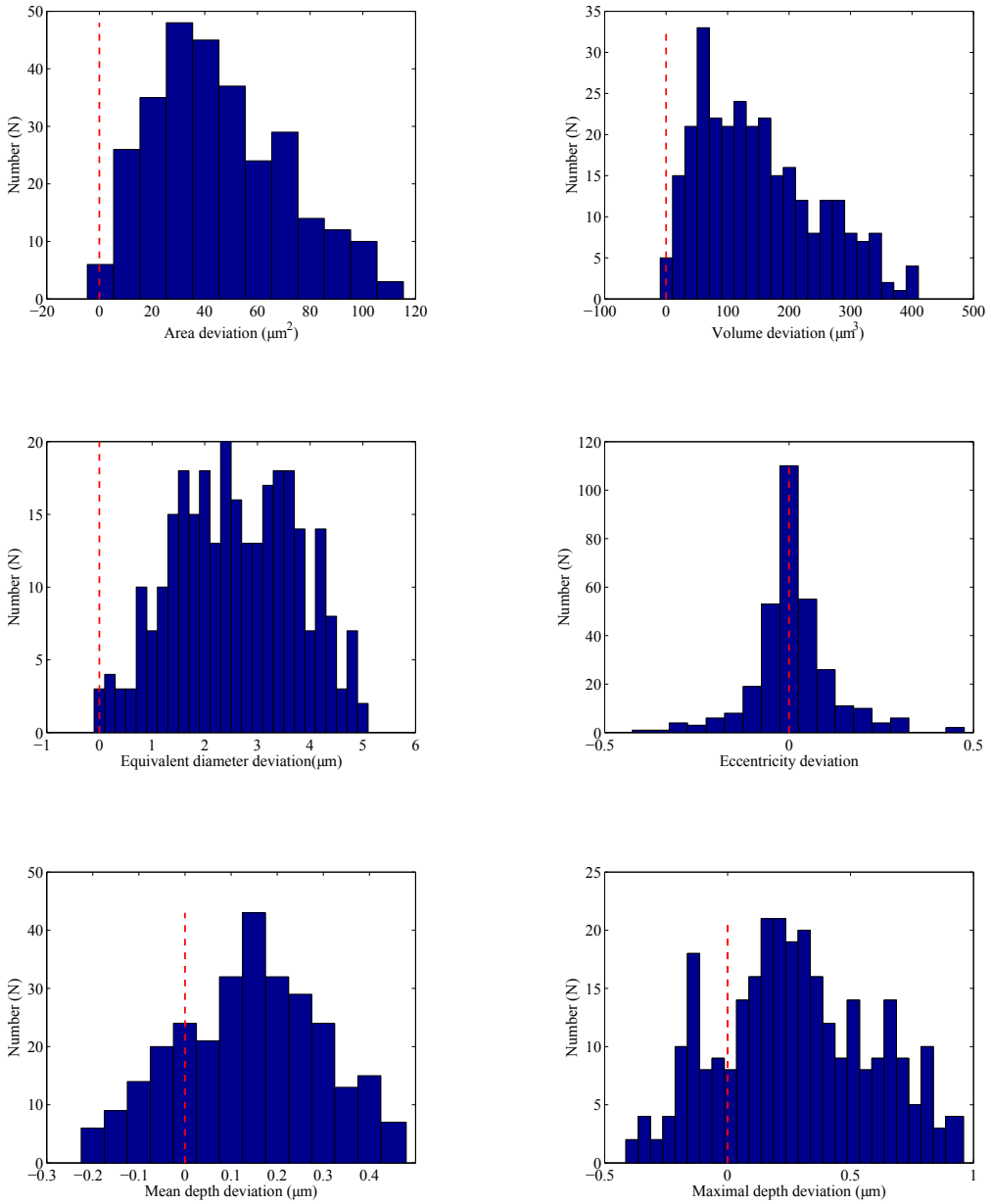

Figure 6: Deviation histogram of different numerical parameters

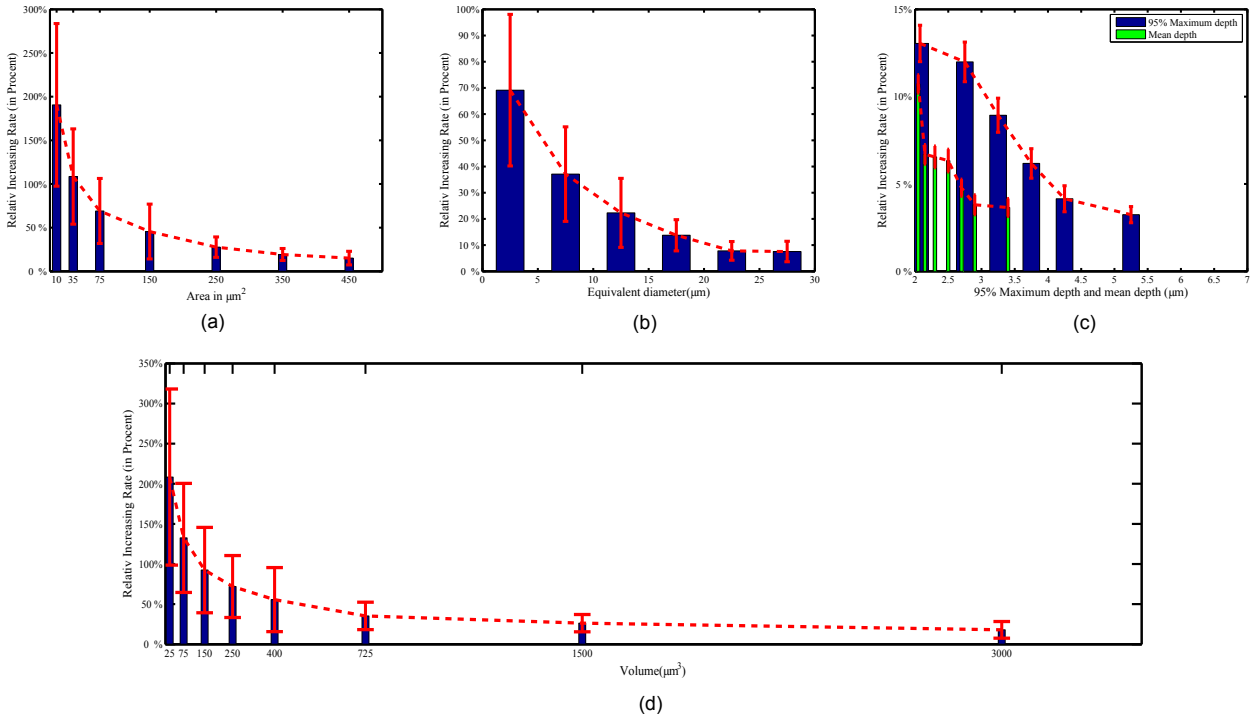

Figure 8: Relation between relative increasing rate and its corresponded numerical parameter

pores with smaller 3D geometry is stronger than on the pores with a larger 3D geometry.

4. Conclusion

This paper has presented a new approach of a multi-resolution characterization to study the impacts of two different sensors on the analysis of a pore's 3D geometry. Some preliminary conclusions can be drawn from the experiments:

1 More details of the local features can be obtained from a lens with a higher resolution due to the reduction of the pixel size.

2 Generally, the impact of using a high resolution lens is greater on the small micro structures than on larger micro structures.

3 The impact degree varies from different numerical parameters. From this study, the lateral correlated parameters are more sensitive to the sensor's resolution than the vertical correlated parameters.

4 Some parameters like eccentricity and roundness of a micro structure can be invariant to sensor's resolution.

Based on the conclusions above, we can take benefit to achieve a fast characterization for porous surfaces. A good case in point is that there is no need to switch to a lens with higher resolution to characterize the eccentricity or roundness of the pores. Another benefit is the estimation of parameter values based on the multi-resolution analysis results. For instance, for the investigation of large pores, which are more than 400 μm^2, we can use 20x lens instead of 50x lens to conduct the data acquisition if certain measurement tolerance for a specific parameter (e.g. 12% for the parameter area according to the Fig. 8a) can be accepted. Thus, not only a faster data acquisition can be achieved, but also the precision of the final data analysis can be guaranteed at the same time.

However, there are also some limitations in this investigation. For instance, different manufacturing processes of porous surfaces were not taken into account to conduct the comparative study. Our experiment was also limited to two sensors: 20x lens and 50x lens. Notwithstanding these limitations, we have demonstrated a new strategy as the first step to deal with the multi-resolution characterization problem. The statistical analysis in Fig. 6 and Fig. 8 have erected the fundamentals for further research, in which the experiment can be extended to using multi-lens acquisition (e.g. three optical lenses) for surface characterization in order to study the relation between different lenses' resolutions and micro structures geometric parameters numerically. A more comprehensive data analysis will be carried out systematically so that a fast characterization based on the data can be finally achieved.

5. Acknowledgements

The authors would like to thank the graduate school "Multi-scale Methods of Interface Coupling" in Leibniz University of Hannover for the financial support.

6. References

[1] G. Barbezat, High performance coatings produced by internal plasma spraying on engine blocks of new generation, Thermal Spray Solutions: Advances in Technology and Application.

[2] G. Barbezat, Advanced thermal spray technology and coating for lightweight engine blocks for the automotive industry, Surface and Coatings Technology 200 (5) (2005) 1990–1993.

[3] J. R. Davis, et al., Handbook of thermal spray technology, ASM international, 2004.

[4] P. Ernst, Friction reduction through thermal spray coatings on cylinder running surfaces of internal combustion engines, iCMCTF 2013 San Diego (May 2013).

[5] P. Ernst, K. Fletcher, Sumebore–thermally sprayed protective coatings for cylinder liner surfaces, in: Proceedings of the 6th International MTZ Conference on Heavy-Duty Onand Off-Highway Engines, Nov, 2011, pp. 15–16.

[6] X. J. Jiang, D. J. Whitehouse, Technological shifts in surface metrology, CIRP Annals-Manufacturing Technology 61 (2) (2012) 815–836.

[7] J. V. Wyngaerd, Combining texture and shape for automatic crude patch registration, in: 3-D Digital Imaging and Modeling, 2003. 3DIM 2003. Proceedings. Fourth International Conference on, IEEE, 2003, pp. 179–186.

[8] D. Zhang, G. Lu, Review of shape representation and description techniques, Pattern recognition 37 (1) (2004) 1–19.

[9] A. Johnson, Spin-images: A representation for 3-d surface matching, Ph.D. thesis, Robotics Institute, Carnegie Mellon University, Pittsburgh, PA (August 1997).

[10] P. J. Besl, N. D. McKay, Method for registration of 3-d shapes, in: Robotics-DL tentative, International Society for Optics and Photonics, 1992, pp. 586–606.

[11] G. Goch, U. Tschudi, J. Pettavel, A universal algorithm for the alignment of sculptured surfaces, CIRP Annals-Manufacturing Technology 41 (1) (1992) 597–600.

[12] T. Lindeberg, Scale-space theory in computer vision, Springer, 1993.

[13] T. Lindeberg, Scale-space for discrete signals, Pattern Analysis and Machine Intelligence, IEEE Transactions on 12 (3) (1990) 234–254.

[14] H. Bay, A. Ess, T. Tuytelaars, L. Van Gool, Speeded-up robust features (surf), Computer vision and image understanding 110 (3) (2008) 346–359.

[15] D. G. Lowe, Distinctive image features from scale-invariant keypoints, International journal of computer vision 60 (2) (2004) 91–110.

[16] K. Mikolajczyk, C. Schmid, Scale & affine invariant interest point detectors, International journal of computer vision 60 (1) (2004) 63–86.